

NJC

Accepted Manuscript



This is an *Accepted Manuscript*, which has been through the Royal Society of Chemistry peer review process and has been accepted for publication.

Accepted Manuscripts are published online shortly after acceptance, before technical editing, formatting and proof reading. Using this free service, authors can make their results available to the community, in citable form, before we publish the edited article. We will replace this *Accepted Manuscript* with the edited and formatted *Advance Article* as soon as it is available.

You can find more information about *Accepted Manuscripts* in the [Information for Authors](#).

Please note that technical editing may introduce minor changes to the text and/or graphics, which may alter content. The journal's standard [Terms & Conditions](#) and the [Ethical guidelines](#) still apply. In no event shall the Royal Society of Chemistry be held responsible for any errors or omissions in this *Accepted Manuscript* or any consequences arising from the use of any information it contains.

ARTICLE

Photofunctional nanocomposites based on the functionalization of metal-organic framework by up/downconversion luminescent nanophosphors

Cite this: DOI: 10.1039/x0xx00000x

Received 00th January 2012,
Accepted 00th January 2012

Chang Liu, Bing Yan*

DOI: 10.1039/x0xx00000x

www.rsc.org/

A novel strategy is demonstrated to construct photofunctional nanocomposites by composing surfactant-capped nanophosphors (upconversion $\text{NaYF}_4:\text{Yb}^{3+},\text{Er}^{3+}/\text{Tm}^{3+}$ and downconversion $\text{LaPO}_4:\text{Ln}^{3+}$ ($\text{Ln} = \text{Ce}, \text{Eu}, \text{Tb}$) nanoparticles) and a zeolitic imidazolate framework (ZIF-8) unit. These nanocomposites show the tunable luminescent performance for different photoactive units or different excitation wavelength. For $\text{NaYF}_4:\text{Yb}^{3+},\text{Er}^{3+}/\text{Tm}^{3+}@ZIF-8$ nanocomposites, they display the luminescence of $\text{NaYF}_4:\text{Yb}^{3+},\text{Er}^{3+}/\text{Tm}^{3+}$ under near infra-red (NIR) 980 nm laser excitation and ZIF-8 under near ultra-violet (NUV) 396 nm excitation, respectively. For $\text{LaPO}_4:\text{Ln}^{3+}$ ($\text{Ln} = \text{Ce}, \text{Eu}, \text{Tb}$)@ZIF-8 nanocomposites, they exhibit emissions of both $\text{LaPO}_4:\text{Ln}^{3+}$ ($\text{Ln} = \text{Ce}, \text{Eu}, \text{Tb}$) and ZIF-8, tuning the different luminescent colors, which does not exist energy coupling between the two emissive centers from each other. These results provide useful data for potential application in optical devices.

Introduction

Metal-organic frameworks (MOFs) are a class of crystalline hybrid materials which synthesized by assembly of metal ions and organic ligands in appropriate conditions^{1,2}. As a permanently microporous materials, MOFs have drawn sustained attention because of their unique properties for two decades. The large specific surface area, ordered crystalline structure, and highly rule-pores make MOFs have a plethora of potential applications, including gas storage, separations, chemical sensing, ion exchange, molecule delivery, catalysis and anything else.³ One of the most important applications is encapsulating a variety of functional species into these peculiar host frameworks to increase or enhance their properties such as luminescence.^{4,5}

zeolitic imidazolate frameworks (ZIFs) are topologically isomorphic with zeolites and belong to a kind of metal-organic frameworks comprised of tetrahedrally-coordinated transition metal ions connected by organic imidazole linkers.⁶ Among ZIF-8 ($\text{Zn}(\text{MeIM})_2$, MeIM = 2-methylimidazole) is a kind of chemically robust and thermally stable material and belongs to the sodalite zeolite-type structure with large cavities and small pore apertures.⁷ ZIF-8 holds an intersecting three-dimensional structural feature, high thermal stability, large pore size and surface area, which are suitable host to compose all kinds of nanoparticles.⁸

Organic-inorganic nanocomposites or nanohybrid materials have high versatility to prepare the tailor-made materials with special chemical and physical properties.⁹ Especially photoactive organic-inorganic nanocomposites have been developed their potential application for such fields as optical materials, device and sensors.¹⁰ Multi-color and white color luminescence are significant for display

and lighting.¹¹ The organic-inorganic nanocomposite materials based with lanthanide species can realize the assembly and composition of different luminescent units in the whole hybrid system,¹² which provides a candidate strategy to reach luminescent control for practical fields such as planar optical amplifiers, solid-state lasers, light-emitting diodes and biolabeling *etc.*¹³ It is worthy pointing out that the crystalline framework is important in the nanocomposite system to further improve the physical and chemical properties of them.¹⁴ Especially some inorganic compounds such as Si, ZnO, TiO_2 , MS ($\text{M} = \text{Zn}, \text{Cd}, \text{Ag}_2\text{S}$), ZnSe *etc.* can be assembled with lanthanide complexes and further realizes the luminescent integration.¹⁵ For nanocomposites based with MOF such as ZIF-8, some efforts are used for composing with all kinds of typical inorganic nanoparticles.¹⁶ Recently some of the luminescent materials (quantum dots, upconversion nanoparticles and lanthanide complex) are encapsulated into MOFs have been reported. Although these materials can be spread into the caves and/or channels of the MOFs because of the little size (some have the molecular level), their products properties are very unstable, easy reunite to quench, high temperature to decompose and readily escape from the channels and caves.¹⁷ Upconversion nanoparticles through lanthanide absorbing a near-infrared excitation shift into a visible light and display high photochemical stability, remarkable light purity, and large anti-Stokes shifts in comparison with semiconducting nanoparticles and organic dyes.¹⁸ On the other hand, rare earth phosphate nanoparticles are also main research object, because of their unique crystal structures, chemical, electronic, and special optical properties.¹⁹ Rare earth phosphate have been proved to process the following applications, such as backlit LCD displays,

plasma panel displays, field-emission displays and new luminescent lamps.

Here we report an assembly strategy that surfactant-capped nanoparticles (upconversion $\text{NaYF}_4:\text{Yb}^{3+},\text{Er}^{3+}/\text{Tm}^{3+}$ and downconversion $\text{LaPO}_4:\text{Ln}^{3+}$ ($\text{Ln} = \text{Ce}, \text{Eu}, \text{Tb}$)) can be covered by a readily synthesized zeolitic imidazolate framework (ZIF-8) through in-situ composing method. The detailed physical characterization and especially the photophysical properties of these nanocomposites are studied.

Experimental section

Chemicals and starting materials

Solutions of $\text{RECl}_3 \cdot x\text{H}_2\text{O}$ ($\text{RE} = \text{Y}, \text{La}, \text{Ce}, \text{Eu}, \text{Gd}, \text{Tb}, \text{Er}, \text{Tm}, \text{Yb}$) in ethanol were obtained by dissolving RE_2O_3 (except Tb_4O_7) in hydrochloric acid (37 %), followed by evaporation and solvation in ethanol, respectively. All the other reagents are analytical pure and purchased from China National Medicines Group.

Chemically pure and highly crystalline ZIF-8 (zeolitic imidazolate frameworks $\text{Zn}(\text{MeIM})_2$, $\text{MeIM} = 2\text{-methylimidazole}$) with the dimension of 30-250 nm was synthesized and characterized according to the reported steps.²⁰ Upconversion nanoparticles doped NaYF_4 or NaGdF_4 (18 % Yb^{3+} , 2 % Er^{3+} or 2 % Tm^{3+}) nanoparticles were synthesized by using the previously reported procedure.²¹ $\text{LaPO}_4:\text{Ln} \cdot x\text{H}_2\text{O}$ ($\text{Ln} = \text{Ce}, \text{Eu}$ or Tb , $x = 0.5\text{-}1$) nanoparticles were carried out according to a slightly modified literature synthesis. $\text{LaPO}_4:\text{Ln} \cdot x\text{H}_2\text{O}$ nanoparticles were synthesized by the liquid–solid–solution (LSS) method.²² Generally, 1.20 g NaOH , 5 ml H_2O , 10 ml ethanol, 5 mL 0.2 M $\text{Ln}(\text{NO}_3)_3 \cdot x\text{H}_2\text{O}$ (aq) solution ($\text{Ln} = \text{Ce}, \text{Eu}, \text{Tb}$ with $\text{Ln}:\text{Ce}/\text{Eu}/\text{Tb} = 19: 1$), 20 mL oleic acid (OA), and 1 mmol Na_3PO_4 were mixed together with vigorous stirring. After stirring for 30 minutes, and transferred into a vial (100 mL). The vial was kept at 120 °C for 10 hrs, and then cooled to room temperature. Then washed by a mixture of chloroform: ethanol (1: 2) three times, and diffused in cyclohexane at room temperature.

surfactant-stabilized upconversion nanoparticles and $\text{LaPO}_4:\text{Ln}^{3+}$ ($\text{Ln} = \text{Ce}, \text{Eu}, \text{Tb}$)

A certain amount of upconversion nanoparticles or $\text{LaPO}_4:\text{Ln}^{3+}$ were dispersed in 10 mL of chloroform. A solution of chloroform of poly vinyl pyrrolidone (PVP 50 mg, $M_w = 10,000$) was added into the above suspension and the mixture was stirred at room temperature for 24 hrs. The PVP-stabilized upconversion nanoparticles and $\text{LaPO}_4:\text{Ln}^{3+}$ were sedimentated with hexane and collected by centrifuging at 10,000 rpm for 5 minutes. The sample was cleaned with chloroform and hexane three times to remove the excess PVP. The PVP-stabilized upconversion nanoparticles and $\text{LaPO}_4:\text{Ln}^{3+}$ were dispersed into methanol.

$\text{NaYF}_4:\text{Yb}^{3+},\text{Er}^{3+}/\text{Tm}^{3+}@ZIF-8$ and $\text{LaPO}_4:\text{Ln}^{3+}@ZIF-8$ ($\text{Ln} = \text{Ce}, \text{Eu}, \text{Tb}$) nanocomposites

Methanol was used as solvent of all the solutions. Generally, 1 ml solution of upconversion nanoparticles or $\text{LaPO}_4:\text{Ln}^{3+}$ nanoparticles under desired concentration was added into a mixed solution of 2-methylimidazole (25 mM) and $\text{Zn}(\text{NO}_3)_2 \cdot 6\text{H}_2\text{O}$ (25 mM). And then the reaction began at room temperature for 24 hrs without stirring or ultrasonic dispersion. The products were collected

by centrifuging at 10,000 rpm for 5 minutes, washed by methanol three times, and vacuum-dried overnight.

$\text{NaYF}_4:\text{Yb}^{3+},\text{Er}^{3+}/\text{Tm}^{3+}@ZIF-8$ and $\text{LaPO}_4:\text{Ln}^{3+}@ZIF-8$ ($\text{Ln} = \text{Ce}, \text{Eu}, \text{Tb}$) nanocomposite thin films²³

The above-obtained upconversion nanoparticles@ZIF-8 and $\text{LaPO}_4:\text{Ln}^{3+}@ZIF-8$ were suspended in 20 mL of tetrahydrofuran (THF) solution, and then 0.50 mL VPD added to the above suspension to mix for 5 hrs at 313 K. Then 1 mL of liquid monomer ethyl methacrylate (EMA) was injected into the above mixture, followed by initiator benzoyl peroxide (BPO). The amount of initiator was 0.4 - 0.5 % of the monomer. The mixed solution was refluxed about 6 hrs at 353 K to get the polymers which were connected through addition polymerization between VPD and EMA under argon atmosphere. The obtained materials were concentrated by using a rotary vacuum evaporator to remove the excess THF, and the ultimate products were viscous liquid. The luminescent polymer thin films of upconversion nanoparticles@ZIF-8 and $\text{LaPO}_4:\text{Ln}^{3+}@ZIF-8$ were prepared by using a Laurell spin-coater to cover the above colloid solution onto a pre-cleaned 1 cm×1 cm ITO glass which was fixed on. The spin rate and spin time were kept at 1000 rpm for 60 s. The solvent was removed by drying the thin films at room temperature after spin-coating.

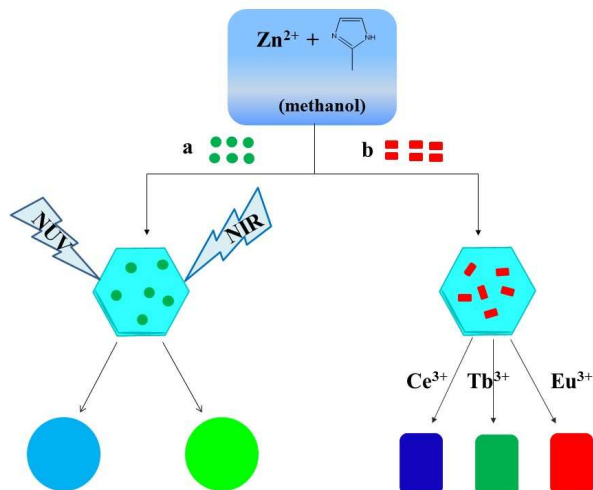
Physical characterization

Powder X-ray diffraction (PXRD) patterns were acquired on a Bruker D8 diffractometer using $\text{CuK}\alpha$ radiation with 40 mA and 40 kV, the data were collected within the 2θ range of 5-65 °. Fourier transform infrared spectra (FTIR) were measured with KBr slices from 4000 to 400 cm^{-1} using a Nexus 912 AO446 infrared spectrum radiometer. Transmission electron microscopy (TEM) was proceed on a JEOL JEM-2010F electron microscope and manipulated at 200 kV. Photoluminescent spectra were obtained on Edinburgh FLS920 spectrophotometer.

Results and discussion

The transmission electron microscopy (TEM) (See Figure S1) and X-ray diffraction patterns (See Figure S2) indicate the sizes and morphology of the nanoparticles, and the functionality of their surfaces was modified with PVP (poly vinyl pyrrolidone) after nanoparticles synthesis. As a kind of nonionic polymer compounds, PVP is the deepest studied, widely used surfactant. During our experiment, PVP can stabilize various nanoparticles in polar solvents, such as methanol that usually used as solvents for ZIF-8 ((zeolitic imidazolate frameworks $\text{Zn}(\text{MeIM})_2$, $\text{MeIM} = 2\text{-methylimidazole}$)) synthesis.²⁴ Scheme 1 shows the preparation process of the nanocomposites. The PVP-nanoparticles@ZIF-8 was synthesized through PVP-protected process described by Lu *et al.*,¹⁶. This strategy involves two steps, the first step of the functionalization of nanoparticle surfaces with PVP and the second step of the crystallization of ZIF-8. ZIF-8 possesses excellent chemical and thermal stability, the sodalite zeolite-type structure, small apertures (3.4 Å), but large cavities (11.6 Å).²⁰ The incorporated nanoparticles were well dispersed in solvents before composing and completely diffused within the ZIF-8 crystals. The as-prepared nanoparticle@ZIF-8 nanocomposites exhibit interesting

optical properties that derive from the above nanoparticles and the other same excellent properties that originate from the ZIF-8.



Scheme 1. Scheme for the preparation of nanocomposites of luminescent nanoparticles and ZIF-8 crystals, (a) upconversion nanoparticles, (b) $\text{LaPO}_4:\text{Ln}^{3+}$ nanoparticles.

The room temperature X-ray diffraction (XRD) patterns from 5 to 65 ° of ZIF-8, $\text{NaYF}_4:\text{Yb}^{3+}/\text{Er}^{3+}$ and $\text{NaYF}_4:\text{Yb}^{3+}/\text{Er}^{3+}@\text{ZIF-8}$ are shown in Figure 1a, which presents the heterostructure of $\text{NaYF}_4:\text{Yb}^{3+}/\text{Er}^{3+}@\text{ZIF-8}$ nanocomposite. The diffraction peaks of $\text{NaYF}_4:\text{Yb}^{3+}/\text{Er}^{3+}@\text{ZIF-8}$ all take agreement well with each value of ZIF-8 and $\text{NaYF}_4:\text{Yb}^{3+}/\text{Er}^{3+}$ as-synthesized. It is indicated that the products have two components of ZIF-8 and $\text{NaYF}_4:\text{Yb}^{3+}/\text{Er}^{3+}$ except for a little difference, which may be influenced by the surfactant PVP adhering on the external of $\text{NaYF}_4:\text{Yb}^{3+}/\text{Er}^{3+}$. The XRD pattern also shows that the existence of $\text{NaYF}_4:\text{Yb}^{3+}/\text{Er}^{3+}$ does not affect the crystal environment of the ZIF-8. Meantime, the peak intensity of ZIF-8 is much stronger than that of $\text{NaYF}_4:\text{Yb}^{3+}/\text{Er}^{3+}$ in their nanocomposite. This is because that little $\text{NaYF}_4:\text{Yb}^{3+}/\text{Er}^{3+}$ were diffused into the large ZIF-8 host and ZIF-8 is the major components of the whole nanocomposite system. The TEM image verifies the results of above-XRD (Figure 1b). And it indicates that the product is composed of the core of $\text{NaYF}_4:\text{Yb}^{3+}/\text{Er}^{3+}$ and the shell of ZIF-8. The particle size of these microcrystals is in the range of 100-120 nm, which is the same as ZIF-8 monocystal.²⁰

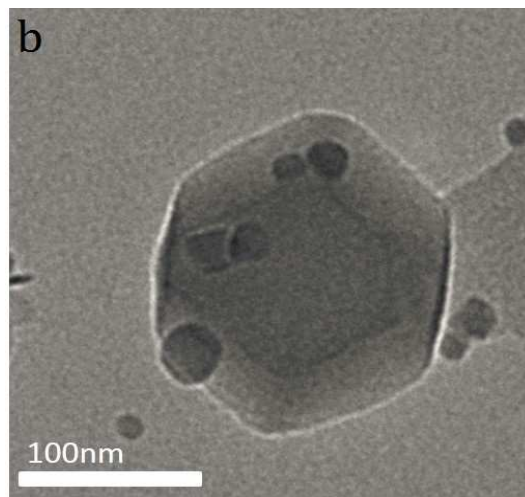
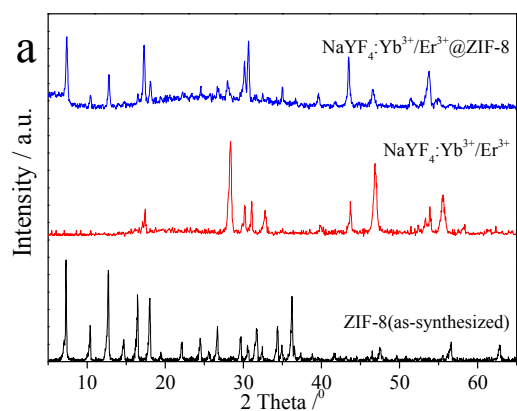


Figure 1 Wide-angle X-ray Diffraction pattern of ZIF-8, $\text{NaYF}_4:\text{Yb}^{3+}/\text{Er}^{3+}$ and $\text{NaYF}_4:\text{Yb}^{3+}/\text{Er}^{3+}@\text{ZIF-8}$ nanocomposite (a), and selected TEM image of $\text{NaYF}_4:\text{Yb}^{3+}/\text{Er}^{3+}@\text{ZIF-8}$ nanocomposite (b).

The selected FT-IR spectra of PVP, $\text{NaYF}_4:\text{Yb}^{3+}/\text{Er}^{3+}$, ZIF-8 and $\text{NaYF}_4:\text{Yb}^{3+}/\text{Er}^{3+}@\text{ZIF-8}$ are shown in Figure 2. The bands of PVP at 2940, 1650 and 1290 cm^{-1} are attributed to C-H, C=O, C-N stretching modes of PVP chains, respectively.²⁵ The C-H bending vibration band appears at 1423 cm^{-1} . $\text{NaYF}_4:\text{Yb}^{3+}/\text{Er}^{3+}$ nanoparticles are synthesized by the above-mentioned LSS method,^{22a} and the bands of 2926, 2855 cm^{-1} are the asymmetric and symmetric stretching vibration of CH_2 group of OA's long alkyl chain. In addition, the asymmetric stretching vibration absorption bands ν (C=O, 1558 cm^{-1}) and ν (C-O, 1455 cm^{-1}) are characteristic of OA's carboxyl group. The bands suggest the existence of residual oleic acid on the $\text{NaYF}_4:\text{Yb}^{3+}/\text{Er}^{3+}$ surface. The band centered at 1384 cm^{-1} of ZIF-8 has relationship to the asymmetric stretching vibration of C-N group, which indicates the presence of MeIM molecules. And it is common phenomenon in the spectrum of $\text{NaYF}_4:\text{Yb}^{3+}/\text{Er}^{3+}@\text{ZIF-8}$ nanocomposite, which distinctly shows that ZIF-8 is the main shell host material of the final nanocomposites. Figure S3 shows the selected FT-IR spectra of PVP, $\text{LaPO}_4:\text{Eu}^{3+}$ nanoparticle, ZIF-8 and $\text{LaPO}_4:\text{Eu}^{3+}@\text{ZIF-8}$ nanocomposite. Similar result feature can be found.

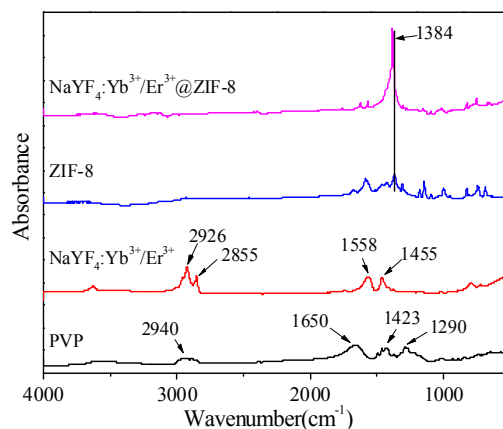


Figure 2 The FT-IR spectra of PVP, $\text{NaYF}_4:\text{Yb}^{3+}/\text{Er}^{3+}$, ZIF-8 and $\text{NaYF}_4:\text{Yb}^{3+}/\text{Er}^{3+}@\text{ZIF-8}$.

The solid-state photoluminescent spectra of nanocomposites NaYF₄:Yb³⁺/Er³⁺@ZIF-8 and LaPO₄:Ln³⁺@ZIF-8 have been studied at room temperature. The upconversion emission spectra of NaYF₄:Yb³⁺/Er³⁺@ZIF-8 are shown in Figure 3a under 980 nm laser diode excitation (power density = 100 W/cm²). The emission spectrum of NaYF₄:Yb³⁺/Er³⁺@ZIF-8 nanocomposite displays three obvious emission bands.²⁶ The green emissions between 510 - 540 nm and 540 - 570 nm are ascribed to the ²H_{11/2} → ⁴I_{15/2} and ⁴S_{3/2} → ⁴I_{15/2} transitions, respectively. Meanwhile a strong red emission can be observed between 640 and 690 nm, which comes from the ⁴F_{9/2} → ⁴I_{15/2} transition of Er³⁺. The ultimate luminescence appears yellow-green color due to a combination of green and red emissions from the Er³⁺ ion. Figure 3b (inserted in Figure 3a) shows a digital photograph of the upconversion luminescence of the sample under the excitation conditions. The spectra of NaGdF₄:Yb³⁺/Er³⁺@ZIF-8 nanocomposite maybe have a little discrepancy compared with NaYF₄:Yb³⁺/Er³⁺@ZIF-8 nanocomposite, because Er³⁺ ions are located in different crystal lattice of NaGdF₄:Yb³⁺/Er³⁺ (Supplementary Figure S4a). The emission bands can be also correctly associated with transitions within the 4f-4f levels of the Er³⁺ ions.

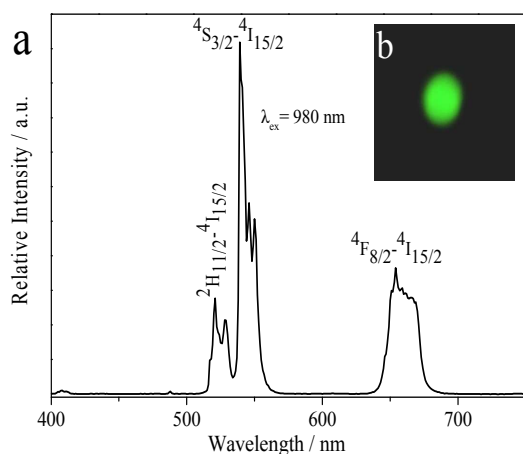


Figure 3 Room-temperature upconversion emission spectrum (a) and digital photograph (b) of NaYF₄:Yb³⁺/Er³⁺@ZIF-8 nanocomposite.

Four main emission bands of Tm³⁺ are observed covering visible-NIR region in the spectrum of NaYF₄:Yb³⁺/Tm³⁺@ZIF-8 nanocomposite (Figure 4a) under excitation of 980 nm laser diode. The tight bands in the blue region of the spectrum between 440 and 490 nm are related to the ¹D₂ → ³F₄ and ¹G₄ → ³H₆ transitions of Tm³⁺. A weak red emission between 640 and 680 nm is assigned to the ¹G₄ → ³F₄ and an intense NIR emission between 750 and 850 nm is ³H₄ → ³H₆ transitions of Tm³⁺, respectively.²⁷ The inset of Figure 4b shows a digital photograph of NaYF₄:Yb³⁺/Tm³⁺@ZIF-8 nanocomposite under the excitation conditions, displaying the light violet-white color for the overlap of blue and red emission in visible region. The upconversion emission spectrum of NaGdF₄:Yb³⁺/Tm³⁺@ZIF-8 nanocomposite is shown in Figure S4b, which presents the similar feature as NaGdF₄:Yb³⁺/Tm³⁺@ZIF-8 nanocomposite.

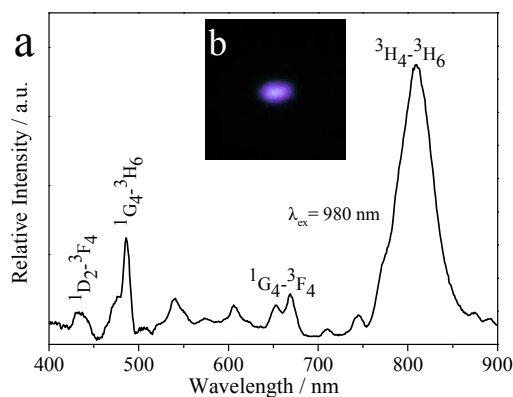


Figure 4 Room-temperature (25 °C) upconversion emission spectrum (a) and digital photograph (b) of NaYF₄:Yb³⁺/Tm³⁺@ZIF-8 nanocomposite.

At ambient temperature, the emission spectrum of NaYF₄:Yb³⁺/Er³⁺@ZIF-8 nanocomposite displays a maximum peak at 450 nm approximately under exciting at 396 nm (Figure 5a). The luminescent feature of shell host ZIF-8 holds a blue emission in visible region under near ultra-violet (NUV) excitation. So NaYF₄:Yb³⁺/Er³⁺@ZIF-8 nanocomposite only shows the luminescence of ZIF-8 unit (blue color). The digital photograph of NaYF₄:Yb³⁺/Er³⁺@ZIF-8 nanocomposite is shown in inserted Figure 5b. ZIFs which have transition-metal ions without unpaired electrons, such as Zn²⁺-like that has *d*¹⁰ formations, can gain linker-based highly emissive materials.²⁸ The luminescent behavior of ZIF-8 is probably ascribed to linker-based because the emission is in the region of the free ligand MeIM molecules (emission at 425 nm). The red shift (460 nm for ZIF-8) is probably related to the coordination effect to form ligand to metal charge transfer (LMCT) from free MeIM molecules to Zn²⁺. Therefore NaYF₄:Yb³⁺/Er³⁺@ZIF-8 nanocomposite can give rise to luminescence both up and down-conversion by selective excitation of near in-fared 980 nm laser and NUV light, respectively, which is interesting for the luminescence color tuning to have application.

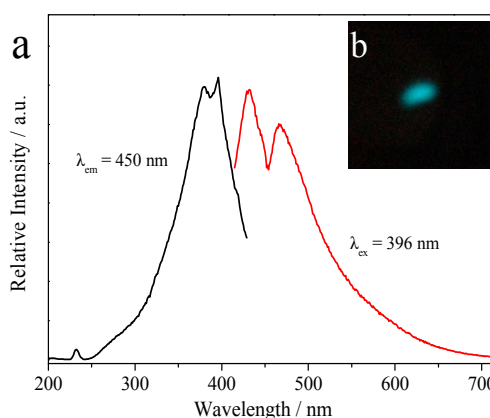


Figure 5 The luminescent excitation and emission spectra (a) and digital photograph (b) NaYF₄:Yb³⁺/Er³⁺@ZIF-8 nanocomposite (λ_{ex} = 396 nm)

Figure 6 shows the luminescent spectrum and digital

photograph of $\text{LaPO}_4:\text{Ce}^{3+}@\text{ZIF-8}$ nanocomposite. For Figure 6a, monitoring by the emission wavelength at 380 nm, the excitation spectrum displays about one broad excitation band at the range of 250 – 350 nm with two prominent peaks with maximum at 280 and 308 nm. This broad band can be attributed to the transitions from the ground state $^2F_{5/2}$ of Ce^{3+} to different crystal field components of the excited Ce^{3+} 5d levels. The corresponding emission spectrum shows a broad band with a maximum at 380 nm (Figure 6a), which may be directly assigned to the parity-allowed 5d \rightarrow 4f electronic transitions of Ce^{3+} ions from the lowest component of the 5d excited state to the spin-orbit components of the ground state. A weak band at around 460 nm in the emission spectrum can be observed, which may be due to the characteristic emission peak of ZIF-8. The final $\text{LaPO}_4:\text{Ce}^{3+}@\text{ZIF-8}$ nanocomposite shows obvious blue emissions under irradiation, whose digital photograph is shown in inserted Figure 6b (blue color).

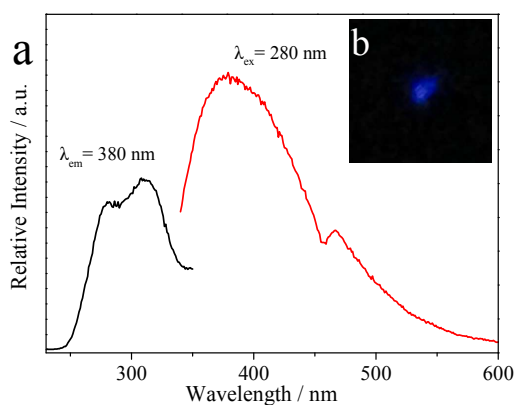


Figure 6 The excitation and emission spectrum (a) and digital photograph by a 280 nm irradiated in dark (b) of $\text{LaPO}_4:\text{Ce}^{3+}@\text{ZIF-8}$ nanocomposite.

The solid-state excitation and emission spectrum of $\text{LaPO}_4:\text{Tb}^{3+}@\text{ZIF-8}$ nanocomposite under room-temperature is presented in Figure 7. The excitation spectrum is collected by monitoring characteristic emission wavelength of Tb^{3+} at 545 nm. A broad band between 300 and 360 nm with the maximum peak of approximately 325 nm is originated from the phosphate host. And another sharp line peak ranged in 360-400 nm is ascribed to Tb^{3+} (4f–4f) direct excitation (See Figure 7a). The corresponding emission spectrum of $\text{LaPO}_4:\text{Tb}^{3+}@\text{ZIF-8}$ nanocomposite is consisted of one strong green band centered at 545 nm and three weak peaks located at 493, 580, and 630 nm, respectively. The former emission line corresponds to the $^5D_4\rightarrow^7F_5$ transition, while the latter are attributed to the $^5D_4\rightarrow^7F_6$, $^5D_4\rightarrow^7F_4$, and $^5D_4\rightarrow^7F_3$ transitions of the Tb^{3+} ions, respectively. Besides, a broad band which is situated at the blue region between 420 and 470 nm, is the emission of ZIF-8. The final luminescence appears light blue in color due to a combination of green and blue emissions from the $\text{LaPO}_4:\text{Tb}^{3+}$ and ZIF-8 respectively. Figure 7b inserted shows the digital photograph of the sample luminescence under the excitation conditions (light blue color). Therefore, the composition of ZIF-8 and $\text{LaPO}_4:\text{Tb}^{3+}$ in polymer hybrids achieve the luminescence tuning.

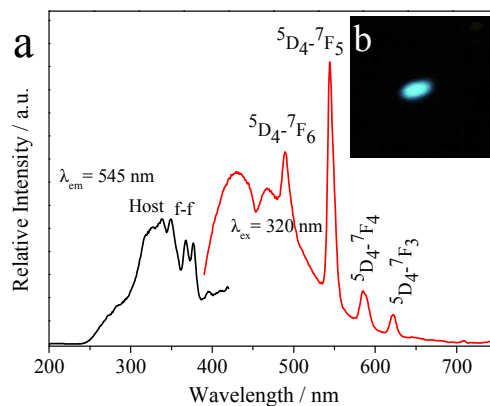


Figure 7 The excitation and emission spectrum (a) and digital photograph by a 320 nm irradiated in dark (b) of the $\text{LaPO}_4:\text{Tb}^{3+}@\text{ZIF-8}$.

The excitation spectra of $\text{LaPO}_4:\text{Eu}^{3+}@\text{ZIF-8}$ nanocomposite are obtained by selecting the emission wavelength of Eu^{3+} at 614 nm (Figure 8a). The little broad excitation bands from 260 to 300 nm with a maximum value of 280 nm which can be observed in the ultraviolet region, is related to the phosphate. The prominent wide excitation bands range in 300-370 nm with maximum 350 nm is originated from the Eu-O LMCT of the core ($\text{LaPO}_4:\text{Eu}^{3+}$). Besides, it is obvious that strong and sharp lines appearing in 370-500 nm range are attributed to the intra-configurational narrow 4f–4f transitions of Eu^{3+} ,²⁹ and especially the strongest excitation peaks are at 393 nm ($^7F_0\rightarrow^5L_6$) and secondly located at 470 nm ($^7F_0\rightarrow^5D_2$), respectively.³⁰ In the emission spectrum, when the excitation wavelength chose at 320 nm, only the red emission of $\text{LaPO}_4:\text{Eu}^{3+}$ is observed with transition ($^5D_0\rightarrow^7F_1$ ($J = 1, 2, 3, 4$)). According to the Judd–Ofelt theory, magnetic dipole transition ($^5D_0\rightarrow^7F_1$) of Eu^{3+} is permitted; electric dipole transition ($^5D_0\rightarrow^7F_2$) is also allowed when Eu^{3+} occupied the site without an inversion center. Meanwhile, the intensity of $^5D_0\rightarrow^7F_1$ transition is not the strongest. The luminescent digital photograph (Figure 8c) under exciting at 320 nm. Comparing the two kinds of excitation spectra of ZIF-8 and $\text{LaPO}_4:\text{Eu}^{3+}$, they have the same excitation bands at 390 nm approximately. So when monitored by the emission wavelength at 393 nm, both of the two materials are displayed in the emission luminescent spectra of $\text{LaPO}_4:\text{Eu}^{3+}@\text{ZIF-8}$ nanocomposite. The blue emissions between 450 and 520 nm was assigned to the ZIF-8, and a dominant red emission was observed between 590 and 700 nm originating from the $\text{LaPO}_4:\text{Eu}^{3+}$ above-mentioned, respectively. The integration luminescence appears warm white in color due to a combination of blue and red emissions from this two materials. The luminescent digital photograph shows in Figure 9d. Therefore, $\text{LaPO}_4:\text{Eu}^{3+}@\text{ZIF-8}$ nanocomposite becomes a novel phosphor which can achieve to emit lights with different colors under selective excitation wavelengths. The photographs of the thin films are exhibited in Figure S5, which shows the transparency of the film. The transparency of $\text{LaPO}_4:\text{Eu}^{3+}@\text{ZIF-8}$ is better than $\text{NaYF}_4:\text{Yb}^{3+}/\text{Er}^{3+}@\text{ZIF-8}$.

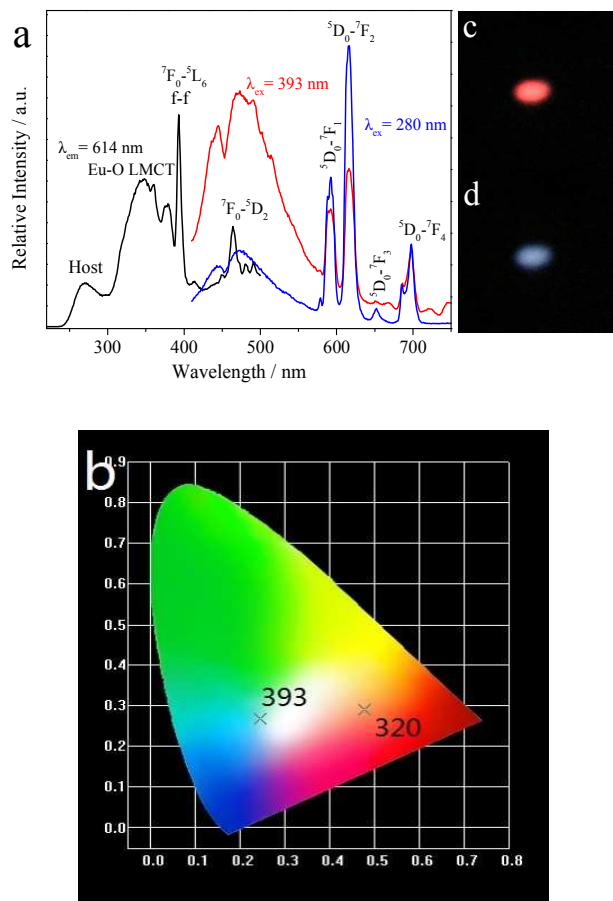


Figure 8 The excitation and emission spectrum (a), the luminescent CIE diagram for the sample with different excitation wavelength (b), and the digital photograph under exciting at 320 nm (c) or 393 nm (d) of $\text{LaPO}_4:\text{Eu}^{3+}@\text{ZIF-8}$ nanocomposite.

Conclusions

In summary, we have demonstrated an effective strategy to prepare photofunctional nanocomposites basing with typical up/downconversion rare earth nanophosphors and a readily assembled MOF material (ZIF-8). $\text{NaYF}_4:\text{Yb}^{3+},\text{Er}^{3+}/\text{Tm}^{3+}@\text{ZIF-8}$ nanocomposites display the luminescence of $\text{NaYF}_4:\text{Yb}^{3+},\text{Er}^{3+}/\text{Tm}^{3+}$ under near infra-red (NIR) 980 nm laser excitation and ZIF-8 under near ultra-violet (NUV) 396 nm excitation, respectively. $\text{LaPO}_4:\text{Ln}^{3+}$ ($\text{Ln} = \text{Ce}, \text{Eu}, \text{Tb}$)@ZIF-8 nanocomposites exhibit emissions of both $\text{LaPO}_4:\text{Ln}^{3+}$ ($\text{Ln} = \text{Ce}, \text{Eu}, \text{Tb}$) and ZIF-8, tuning the different luminescent colors. These nanocomposites show the tunable luminescent performance for different photoactive units or different excitation wavelength, which provide useful data for potential application in optical devices.

Acknowledgements

This work was supported by the National Natural Science Foundation of China (91122003) and Developing Science Funds of Tongji University.

Notes and references

Department of Chemistry, Tongji University, Shanghai 200092, China.

Fax: +86-21-65982287; Tel: +86-21-65984663;

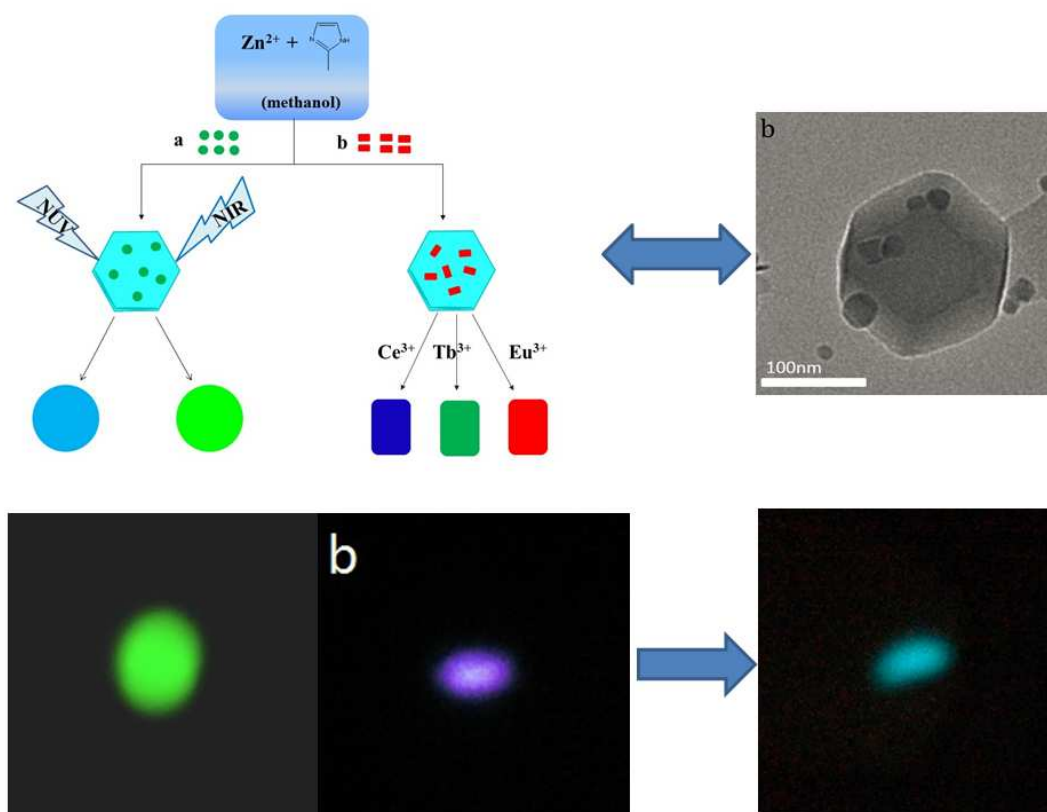
E-mail: byan@tongji.edu.cn

Electronic Supplementary Information (ESI) available: Selected TEM images and X-ray diffraction patterns of the fluoride and phosphate nanocrystals, the selected FT-IR spectra of nanocomposite, up-conversion emission spectra of fluoride nanocrystals and selected photographs of the transparent thin films. See DOI: 10.1039/b000000x/

- (a) O. M. Yaghi, M. O'Keeffe, N. W. Ockwig, H. K. Chae, M. Eddaoudi and J. Kim, *Nature*, 2003, **423**, 705; (b) M. Kurmoo, *Chem. Soc. Rev.*, 2009, **38**, 135; (c) S. Natarajan and P. Mahata, *Chem. Soc. Rev.*, 2009, **38**, 2304.
- (a) S. Horike, S. Shimomura and S. Kitagawa, *Nat Chem*, 2009, **1**, 695; (b) O. Shekhah, J. Liu, R. A. Fischer and Ch. Woll, *Chem. Soc. Rev.*, 2011, **40**, 1081; (c) A. Betard and R. A. Fischer, *Chem. Rev.*, 2012, **112**, 1055.
- (a) J. Lee, O. K. Farha, J. Roberts, K. A. Scheidt, S. T. Nguyen and J. T. Hupp, *Chem Soc Rev*, 2009, **38**, 1450; (b) B. L. Chen, S. C. Xiang and G. D. Qian, *Acc. Chem. Res.*, 2010, **43**, 1115; (c) J. D. Rocca, D. Liu and W. B. Lin, *Acc. Chem. Res.*, 2011, **44**, 957.
- (a) H. K. Chae, D. Y. Siberio-Perez, J. Kim, Y. Go, M. Eddaoudi, A. J. Matzger, M. O'Keeffe and O. M. Yaghi, *Nature*, 2004, **427**, 523; (b) Z. H. Xiang, Z. Hu, D. P. Cao, W. T. Yang, J. M. Lu, B. Y. Han and W. C. Wang, *Angew Chem Int Edit*, 2011, **50**, 491.
- (a) L. E. Kreno, K. Leong, O. K. Farha, M. Allendorf, R. P. Van Duyne and J. T. Hupp, *Chem. Rev.*, 2012, **112**, 1105; (b) P. Horcajada, R. Gref, T. Baati, P. K. Allan, G. Maurin, P. Couvreur, G. Ferey, R. E. Morris and C. Serre, *Chem. Rev.*, 2012, **112**, 1232.
- (a) O. M. Yaghi, M. O'Keeffe, N. W. Ockwig, H. K. Chae, M. Eddaoudi and J. Kim, *Nature*, 2003, **423**, 705; (b) H. Hayashi, A. P. Cote, H. Furukawa, M. O'Keeffe and O. M. Yaghi, *Nat. Mater.*, 2007, **6**, 501; (c) X. C. Huang, Y. Y. Lin, J. P. Zhang and X. M. Chen, *Angew. Chem., Int. Ed.*, 2006, **45**, 1557.
- (a) J. Cravillon, S. Münzer, S. J. Lohmeier, A. Feldhoff, K. Huber and M. Wiebcke, *Chem. Mater.*, 2009, **21**, 1410; (b) H. Bux, F. Y. Liang, Y. S. Li, J. Cravillon, M. Wiebcke and J. Caro, *J. Am. Chem. Soc.*, 2009, **131**, 16000; (c) S. R. Venna and M. A. Carreon, *J. Am. Chem. Soc.*, 2010, **132**, 76.
- (a) R. Ostermann, J. Cravillon, C. Weidmann, M. Wiebcke and B. M. Smarsly, *Chem. Commun.*, 2011, **47**, 442; (b) J. F. Yao, D. H. Dong, D. Li, L. He, G. S. Xu and H. T. Wang, *Chem. Commun.*, 2011, **47**, 2559; (c) G. Lu, S. Z. Li, Z. Guo, O. K. Farha, B. G. Hauser, X. Y. Qi, Y. Wang, X. Wang, S. Y. Han, X. G. Liu, J. S. DuChene, H. Zhang, Q. C. Zhang, X. D. Chen, J. Ma, S. C. J. Loo, W. D. Wei, Y. H. Yang, J. T. Hupp and F. W. Huo, *Nat. Chem.* 2012, **4**, 310.
- (a) A. Maliakal, H. Katz, P. M. Cotts, S. Subramoney and P. Mirau, *J. Am. Chem. Soc.*, 2005, **127**, 14655; (b) M. Mamak, G. S. Metraux, S. Petrov, N. Coombs, G. A. Ozin and M. A. Green, *J. Am. Chem. Soc.*, 2003, **125**, 5161; (c) K. Binnemans, *Chem. Rev.*, 2009, **109**, 4283; (d) L. D. Carlos, R. A. S. Ferreira, V. D. Bermudez and S. J. L. Ribeiro, *Adv. Mater.*, 2009, **21**, 509.
- (a) L. D. Carlos, R. A. S. Ferreira, V. D. Bermudez and S. J. L. Ribeiro, *Adv. Mater.*, 2009, **21**, 509; (b) K. Binnemans, *Chem. Rev.*, 2009, **109**, 4283.
- (a) S. Sivakumar, F. C. J. M van Veggel and M. Raudsepp, *J. Am. Chem. Soc.*, 2005, **127**, 12464; (b) D. Zhao, S. J. Seo and B. S. Bae, *Adv. Mater.*, 2007, **19**, 3473; (c) W. Ki and J. Li, *J. Am. Chem. Soc.*, 2008, **130**, 8114; (d) M. S. Wang, S. P. Guo, Y. Li, L. Z. Cai, J. P. Zou, G. Xu, W. W. Zhou, F. K. Zheng and G. C. Guo, *J. Am. Chem. Soc.*, 2009, **131**, 13572.
- (a) J. Cuan and B. Yan, *Dalton Trans.*, 2013, **42**, 14230; (b) J. Cuan and B. Yan, *RSC Adv.*, 2013, **3**, 20077; (c) J. Cuan and B. Yan,

- Microp. Mesop. Mater.*, 2014, **183**, 9; (d) J. Cuan and B. Yan, *RSC Adv.*, 2014, **4**, 1735.
- 13 (a) J. C. G. Buenzli and C. Piguat, *Chem. Rev.*, 2002, **102**, 1897; (b) M. D. Senarath-Yapa, S. Phimphivong, J. W. Coym, M. J. Wirth, C. A. Aspinwall and S. S. Saavedra, *Langmuir*, 2007, **23**, 12624; (c) K. M. Lee, K. W. Cheah, B. L. An, M. L. Gong and Y. L. Liu, *Appl. Phys. A: Mater. Sci. Proc.*, 2005, **80**, 337.
- 14 (a) Y. F. Shao and B. Yan, *Dalton Trans.*, 2012, **41**, 7423; (b) Y. F. Shao, B. Yan and Z. Y. Jiang, *RSC Adv.*, 2012, **2**, 9192; (c) B. Yan and Y. F. Shao, *RSC Adv.*, 2014, **4**, 3318.
- 15 (a) Y. Zhao and B. Yan, *Dalton Trans.*, 2012, **41**, 5334; (b) Y. Zhao and B. Yan, *J. Coll. Interf. Sci.*, 2013, **395**, 145; (c) Q. P. Li and B. Yan, *RSC Adv.*, 2012, **2**, 10840.
- 16 G. Lu, S. Z. Li, Z. Guo, O. K. Farha, B. G. Hauser, X. Y. Qi, Y. Wang, X. Wang, S. Y. Han, X. G. Liu, J. S. DuChene, H. Zhang, Q. C. Zhang, X. D. Chen, J. Ma, S. C. J. Loo, W. D. Wei, Y. H. Yang, J. T. Hupp and F. W. Huo, *Nat. Chem.*, 2012, **4**, 310.
- 17 (a) M. Meilikhov, K. Yusenko, D. Esken, S. Turner, G. Van Tendeloo and R. A. Fischer, *Eur. J. Inorg. Chem.*, 2010, 3701; (b) P. Falcaro, A. J. Hill, K. M. Nairn, J. Jasieniak, J. I. Mardel, T. J. Bastow, S. C. Mayo, M. Gimona, D. Gomez, H. J. Whitfield, R. Ricco, A. Patelli, B. Marmiroli, H. Amenitsch, T. Colson, L. Villanova and D. Buso, *Nat. Commun.*, 2011, **2**, 237.
- 18 (a) F. Auzel, *Chem. Rev.*, 2004, **104**, 139; (b) J. F. Suyver, A. Aebischer, D. Biner, P. Gerner, J. Grimm, S. Heer, K. W. Kramer, C. Reinhard and H. U. Gudel, *Opt. Mater.*, 2005, **27**, 1111.
- 19 (a) G. Blasse, *J. Alloys Compds.* 1995, **225**, 529; (b) J. A. Dorman, J. H. Choi, G. Kuzmanich and J. P. Chang, *J. Phys. Chem. C*, 2012, **116**, 12854.
- 20 K. S. Park, Z. Ni, A. P. Cote, J. Y. Choi, R. D. Huang, F. J. Uribe-Romo, H. K. Chae, M. O'Keeffe and O. M. Yaghi, *Proc. Natl. Acad. Sci. U. S. A.*, 2006, **103**, 10186.
- 21 F. Wang, Y. Han, C. S. Lim, Y. H. Lu, J. Wang, J. Xu, H. Y. Chen, C. Zhang, M. H. Hong and X. G. Liu, *Nature*, 2010, **463**, 1061.
- 22 (a) X. Wang, J. Zhuang, Q. Peng and Y. D. Li, *Nature*, 2005, **437**, 121; (b) L. X. Yu, H. W. Song, S. Z. Lu, Z. X. Liu, L. M. Yang and X. G. Kong, *J. Phys. Chem. B*, 2004, **108**, 16697.
- 23 (a) B. Brauer, D. R. T. Zahn, T. Ruffer and G. Salvan, *Chem. Phys. Lett.*, 2006, **432**, 226; (b) D. W. Schubert and T. Dunkel, *Mater. Res. Innov.*, 2003, **7**, 314.
- 24 Z. Q. Li and Y. Zhang, *Angew Chem Int Edit*, 2006, **45**, 7732-7735.
- 25 Y. Borodko, S. E. Habas, M. Koebel, P. D. Yang, H. Frei and G. A. Somorjai, *J Phys Chem B*, 2006, **110**, 23052-23059.
- 26 J. C. Boyer, F. Vetrone, L. A. Cuccia and J. A. Capobianco, *J. Am. Chem. Soc.*, 2006, **128**, 7444-7445.
- 27 M. Pollnau, D. R. Gamelin, S. R. Luthi, H. U. Gudel and M. P. Hehlen, *Phys. Rev. B*, 2000, **61**, 3337.
- 28 S. Liu, Z. H. Xiang, Z. Hu, X. P. Zheng and D. P. Cao, *J. Mater. Chem.*, 2011, **21**, 6649-6653.
- 29 S. Park, Z. Zhen and D. H. Park, *Mater. Lett.*, 2010, **64**, 1861.
- 30 M. D. Regulacio, M. H. Pablico, J. A. Vasquez, P. N. Myers, S. Gentry, M. Prushan, S. W. Tam-Chang and S. L. Stoll, *Inorg. Chem.*, 2008, **47**, 1512.

TOC



A novel strategy is demonstrated to construct photofunctional nanocomposites by composing surfactant-capped nanophosphors (upconversion $NaYF_4:Yb^{3+},Er^{3+}/Tm^{3+}$ and downconversion $LaPO_4:Ln^{3+}$ ($Ln = Ce, Eu, Tb$) nanoparticles) and a zeolitic imidazolate framework (ZIF-8) unit. These nanocomposites show the tunable luminescent performance for different photoactive units or different excitation wavelength. These results provide useful data for potential application in optical devices.